Advanced Science

ADVANCED SCIENCE Open Access
www.advancedscience.com

RESEARCH ARTICLE OPEN ACCESS

Transmission of Radio-Frequency Waves and Nuclear Magnetic Resonance in Lanthanum Superhydrides

Dmitrii V. Semenok[1] | Florian Bärtl[2,3] | Di Zhou[1] | Toni Helm[2,4] | Sven Luther[2] | Joachim Wosnitza[2,3] | Ivan A. Troyan[5] | Viktor V. Struzhkin[6,7] | Hannes Kühne[2]

[1]Center For High Pressure Science & Technology Advanced Research, Beijing, China | [2]Hochfeld-Magnetlabor Dresden (HLD-EMFL) and Würzburg-Dresden Cluster of Excellence ctd.qmat, Helmholtz-Zentrum Dresden-Rossendorf, Dresden, Germany | [3]Institut für Festkörper- und Materialphysik, Technische Universität Dresden, Dresden, Germany | [4]Max Planck Institute for Chemical Physics of Solids, Dresden, Germany | [5]A.V. Shubnikov Institute of Crystallography of the Kurchatov Complex of Crystallography and Photonics, Moscow, Russia | [6]Shanghai Key Laboratory of Material Frontiers Research in Extreme Environments (MFree), Shanghai Advanced Research in Physical Sciences (SHARPS), Shanghai, China | [7]Center For High Pressure Science & Technology Advanced Research, Shanghai, China

Correspondence: Dmitrii V. Semenok (dmitrii.semenok@hpstar.ac.cn) | Viktor V. Struzhkin (viktor.struzhkin@hpstar.ac.cn) | Hannes Kühne (h.kuehne@hzdr.de)

Received: 17 October 2025 | **Revised:** 28 January 2026 | **Accepted:** 29 January 2026

Keywords: high pressure | NMR | radio-frequency methods | superconductivity | superhydrides

The discovery of near-room-temperature superconductivity in the lanthanum hydride LaH_{10} has revolutionized this research field. However, the need to use diamond anvils for the synthesis of hydride superconductors severely limits the experimental techniques to study these materials. Nuclear magnetic resonance (NMR) is one of the key methods for probing spin systems of superconductors. Here we show how ^{1}H NMR can be realized in diamond anvil cells to study lanthanum polyhydrides at pressures up to 165 GPa. In the newly discovered superhydride LaH_{12}, we observed a pronounced suppression of the ^{1}H NMR signal intensity below T_c^{onset} = 260 K in a magnetic field of 7 T, corresponding to the screening of the radio-frequency pulses. Below the critical temperature, all ^{1}H NMR characteristics, including the nuclear spin-lattice relaxation rate $1/T_1T$, exhibit pronounced features that may be associated with superconductivity. In zero field, the radio-frequency signal transmission shows a pronounced drop below $T_c^{onset} \approx$ 267–279 K, indicating the very beginning of the transition in the most ideal microcrystals. A description of the $1/T_1T$ data with an exponential form allows the estimation of the superconducting gap $\Delta(0)$ = 427–671 K (corresponding to 36.8–57.8 meV), and the ratio $R_\Delta = 2\Delta(0)/k_BT_c$ between 3.76 and 5.16 in the synthesized polyhydride.

1 | Introduction

Superhydrides are a rapidly developing class of hydrogen-rich compounds that have attracted considerable attention in the field of condensed-matter physics due to their remarkable superconducting properties. The experimental discovery of high-temperature superconductivity (SC) in H_3S (T_c^{max} = 203 K [1]), LaH_{10} (T_c^{max} = 250 K [2, 3]), ThH_{10} (T_c^{max} = 161 K [4]), YH_6 (T_c^{max} = 224-226 K [5, 6]), CeH_{10} (T_c^{max} = 115 K [7]), and many other polyhydrides [8, 9], was preceded by numerous theoretical predictions [10–13], intensive development of computer programs (for example, Quantum Espresso [14, 15], VASP [16], USPEX [17, 18], CALYPSO [19], AIRSS [20]), and ab initio methods for calculating superconducting properties (for instance, SCDFT [21, 22] and SSCHA [23]). Eventually, it has opened new avenues for fundamental and applied studies. Particularly, the search for room-temperature superconductors and the development of magnetic field sensors, diodes, and

Dmitrii V. Semenok, Florian Bärtl, and Di Zhou contributed equally to this work.

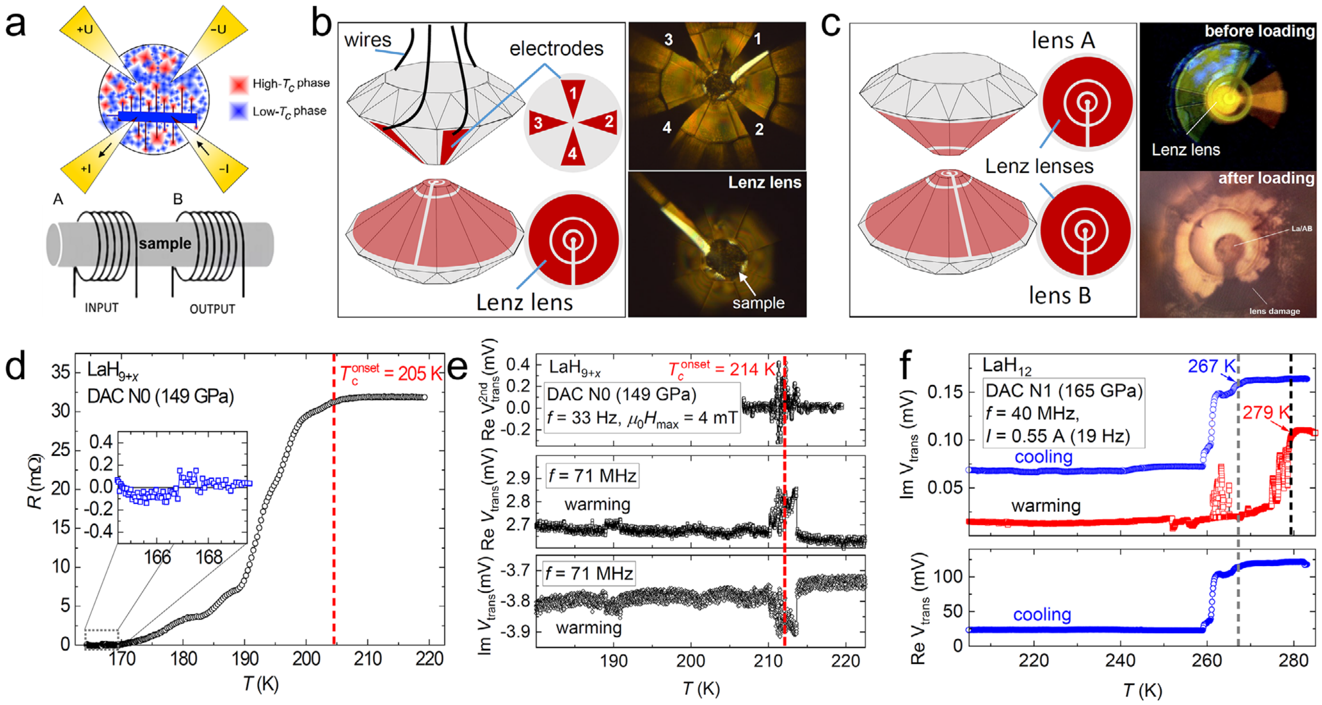

FIGURE 1 | Electrical resistance and RF transmission of lanthanum superhydrides, synthesized from La and NH_3BH_3 in the DACs N0 and N1. (a) Sketch of a possible distribution of high-T_c and low-T_c superconducting phases in a hydride sample, which complicates the detection of high-T_c SC using a four-electrode van der Pauw circuit. At the same time, only the low-T_c transition may be detected due to the presence of a homogeneous segment of the corresponding phase (marked in blue) between the electrodes. Also shown is a scheme of RF diagnostics, employing a transformer circuit (coil A is input, coil B is output). (b) Schematic diagram of the DAC N0, containing a four-electrode circuit for transport measurements and a Lenz lens for RF transmission measurements. Right: Images of the DAC culet, loaded sample, electrode system and Lenz lens. (c) Schematic diagram of the DAC N1, containing two Lenz lenses for RF transmission measurements and NMR studies. Right: Images of the anvil culet with sputtered Lenz lenses before and after loading and compression to 165 GPa. (d) Electrical resistance (current is 1 mA, DC) as a function of temperature for a sample of lanthanum hydride in DAC N0 at 120 GPa. Inset: residual resistance of the sample below 170 K. (e) Real (Re) and imaginary (Im) components of the RF signal passing through the DAC N0 sample in transformer mode. The carrier frequency is 71 MHz. Top panel: Directly demodulated RF signal of the second harmonic of the low-frequency modulating field (33 Hz, $B_{max} \approx 4$ mT). (f) High-frequency (40 MHz) study of the DAC N1 at 165 GPa. Real and imaginary components of the receiving coil signal in the cooling cycle. The superconducting transition of the sample in DAC N1 starts around 267 K. A thermal hysteresis (about 10 to 12 K) in the system as exemplified by the imaginary (Im) components of the receiving coil signal. The thermometer was glued to the outside of DAC N1.

memory elements based on superhydrides gave a new impetus to the research efforts [24–26]. Unfortunately, polyhydride samples are often inhomogeneous [27, 28]. A comprehensive study of SC in such inhomogeneous samples is problematic due to the presence of several crystallographic phases, including metastable ones [29], with very different critical temperatures (Figure 1a). Indeed, impurity phases or grains, separated from the probing current trajectories by non-superconducting lower hydrides or insulating shells of higher polyhydrides, cannot be identified by standard four-probe transport measurements (Figure 1a). Such grains with varying superconducting properties may be responsible for broadened or steplike transitions in the temperature dependence of the resistance, hardly distinguishable inhomogeneous sample quality, or stress distributions. Detection methods based on volume-penetrating electromagnetic fields can be suitable probing techniques in this situation. Radiofrequency (RF) contactless measurements [30, 31] and nuclear magnetic resonance (NMR) spectroscopy [32] allow to overcome this problem and detect SC in inhomogeneous samples under pressure.

NMR spectroscopy is based on the coherent manipulation of the nuclear spin system in a material [33, 34]. It can be employed to probe the magnetic hyperfine fields, originating from the electronic subsystem. Thus, it is very sensitive to the static electronic spin susceptibility and low-energy excitations of the electronic system. The shape of an NMR spectrum, its broadening and frequency shift depend on the magnetic interactions of the nuclear moments with their environment [35]. ^{27}Al-NMR spectroscopy played a major role in confirming the Bardeen–Cooper–Schrieffer (BCS) theory of SC [36]. Moreover, Redfield, Anderson, Hebel, and Slichter discovered that at temperatures below the superconducting critical temperature (T_c), there is a maximum of the ^{27}Al spin-lattice relaxation rate $1/T_1$ (the Hebel-Slichter peak) in aluminum [37–39]. Measurements of $1/T_1$ at temperatures well below T_c yield an exponential decrease of $1/T_1$ with temperature in the case of a full superconducting gap. In metals, the NMR frequency shift (also called Knight shift [40]) and the spin-spin relaxation rate $1/T_2$ are independent of temperature [41], whereas $1/T_1$ is proportional to temperature (known as Korringa relation [42]). A distinctive feature of a superconducting transition is a sharp decrease of the relaxation rate $1/T_1T$ due to the opening of the superconducting gap.

Since the beginning of research on superhydrides, it was suggested that they were the most prominent representatives of BCS superconductors [1]. NMR spectroscopy is a powerful tool for studying the nature of the normal and superconducting ground states. Therefore, it can help to obtain information on the superconducting gap in the polyhydrides. However, NMR studies on these materials face a major experimental challenge—the tiny sample space of a diamond anvil cell (DAC), which is required to create the necessary pressures of over 1 million atmospheres (100 GPa). Here, the comparably high sensitivity of NMR spectroscopy to the ^{1}H isotope, the sublattice of which plays a major role in the SC of hydrides [8], is very beneficial. Fortunately, an approach has recently been developed that allows the detection of ultra-small samples via conventional solid-state NMR techniques, using focusing Lenz lenses deposited on diamond anvils [32, 43, 44]. Lower hydrides of FeH [45, 46], Cu_2H [47], YH_3 [32], LaH_3 [44], and molecular hydrogen [48, 49], have previously been studied at pressures up to 220 GPa. Below, we will demonstrate that the same Lenz lenses also prove to be a very efficient tool for studying the surface impedance of superhydride samples. Unlike NMR, within this RF transmission method, two Lenz lenses are used separately as excitation (A) and detection (B) microcoils of an RF transformer (Figure 1a).

In this work, we applied RF transmission and ^{1}H NMR techniques to study lanthanum superhydrides, synthesized from La or $LaH_{\sim 3}$ and ammonia borane (NH_3BH_3) in five DACs (labeled as “N0-N4”) at different pressures up to 165 GPa. We were able to study the ^{1}H NMR signal of various lanthanum polyhydrides and observed a transition that was probably of a superconducting nature, stemming from the newly discovered LaH_{12}, yielding a T_c^{onset} above 267 K. This is confirmed by an abrupt change in the RF surface impedance and a sharp drop of the ^{1}H NMR spin-lattice relaxation rate. In our interpretation, superconductivity is the primary hypothesis explaining the phenomena observed in the NMR and RF experiments. The high density of high-T_c superconducting hydrides in the La-H system under pressure, as well as previous transport [3, 50] and magnetic measurements [51], make this hypothesis highly plausible.

2 | Results and Discussion

2.1 | Combined DAC with Electrodes and Lenz Lens

Although the RF method of measuring the surface impedance has been known since 1989 [30], and has been widely used to probe superconducting transitions [31, 52], it has not been applied in combination with Lenz lenses [53] for high-pressure studies. To bridge this gap, in the first (calibration) experiment utilizing the DAC N0 (Figure 1a–e), we used two detection systems simultaneously: a classical four-probe van der Pauw resistance measurement circuit was deposited on one diamond anvil, while a simple single-stage Ta/Au Lenz lens (Figure 1b) was sputtered onto the opposite anvil. After laser heating of La microparticles loaded with ammonia borane (NH_3BH_3) at 149 GPa, the pressure in the DAC dropped to 120 GPa, and the four-contact measurements showed a pronounced resistance drop starting below T_c^{onset} = 205 K (Figure 1d). This T_c is in good agreement with previous studies of the La superhydrides [54, 55]. The result of our synthesis may correspond to the hexagonal polyhydride $P6_3/mmc$-LaH_{9-10} [56, 57] or low-symmetry (e.g., $C2/m$ [54, 58]) LaH_{9+x} (x = ± 1) with a partially molecular hydrogen sublattice [59]. A detailed description of the preparation and characteristics of the sample in DAC N0 is given in the Table S1.

Using any electrode pair of the DAC N0 as an RF antenna and the Lenz lens with a surrounding, macroscopic single-turn coil as a receiver (Figures S1 and S2) allowed us to detect a sharp change in the surface impedance of the sample in the real and imaginary components of the RF signal. This corresponds to a SC transition with an onset at 212 to 214 K (Figure 1e). We detected such steps or jumps of the transmitted RF signal using various frequencies between 0.2 and 71 MHz (Figure 1e; Figure S3), confirming the reproducibility. For additional verification, we used the double-modulation technique, similar to that proposed by Timofeev in 2002 [31]. As shown in the top panel of Figure 1e, placing the sample in a weak ($B_{max} \approx 4$ mT) oscillating magnetic field with a frequency of 33 Hz leads to a pronounced feature in the second harmonic (66 Hz) of the directly demodulated RF signal. This feature emerges simultaneously with the jump in the transmitted RF signal, because the magnetic field suppresses SC, regardless of the sign of the magnetic induction B_z.

The T_c observed by the RF method is somewhat higher than T_c^{onset}, detected my means of the resistance measurements. This is because the high-frequency field penetrates the entire volume occupied by the LaH_{9+x} sample, and not only the space between electrodes, as in the case of the four-electrode circuit. That is why it is possible to detect superconducting phases with the highest T_c regardless of how far they are from the electrodes. Note that reducing the carrier frequency to 0.2–1 MHz also allows for reliable detection of the signal of only the “main” superconducting phases, located near the electrodes, with T_c at about 180 to 190 K (Figure S3). Further radio-frequency transmission tests using MgB_2, NbTi, Bi2212, YBCO, REBCO, $La_{3-x}Nd_xNi_2O_7$ (La,Ce)H_{10-12}, and (La,Sc)H_x can be found in the Refs. [60–63].

2.2 | RF Detection of Superconductivity with Two Lenz Lenses

After successful testing of the contactless RF detection method using Lenz lenses (DAC N0), we prepared DACs containing two Lenz lenses as indicated in Figure 1c (see Supporting Information) for combined RF transmission and ^{1}H NMR studies. We performed experiments with four high-pressure DACs (pressure is given in brackets): DAC N1 (165 GPa), N2 (147 GPa), N3 (87 GPa), and N4 (19 GPa). The samples in the DACs N1 and N2 were obtained by infrared laser heating of metallic La in an NH_3BH_3 environment, while the samples N3 and N4 were obtained by heating of LaH_{3-x} with NH_3BH_3 under pressure. We performed the laser heating at the ID27 beamline of the European Synchrotron Radiation Facility (ESRF). The most interesting results were obtained for the samples N1 and N3, synthesized in symmetric BX-90 mini cells [64], equipped with diamond anvils with a culet diameter of 75 μм. One to two micrometers thick copper or silver films, sputtered onto the diamond anvils, were used for the Lenz lenses [53] (Figure 1c; Figure S1). As we will demonstrate in the next paragraph, the sample in DAC N1 is best described by the formula LaH_{12}. Detailed information on the DAC designs and preparation is given in the Table S1.

First, we performed RF transmission measurements of the sample in DAC N1 at 165 GPa, employing a high-frequency transformer formed by the two Lenz lenses. As can be seen in Figure 1f (as well as in Figure S4), the RF signal transmission exhibits main features at 267 to 279 K, which appear in both the amplitude and phase of the output signal of the RF transformer for various frequencies (40, 150, and 200 MHz). This behavior is accompanied by the appearance of a second harmonic at the frequency of the external modulation field (Figure S4). Another small feature in the RF transmission occurs as well at 248 to 252 K, which probably corresponds to a LaH_{10} impurity (Figure S5). Previous works on lanthanum [3, 50, 51, 65] and lanthanum-scandium [26] hydrides indeed evidenced an additional step-like drop in the electrical resistance, setting in at temperatures between 265 and 279 K or even above. However, such a high T_c could not be attributed to any known La hydride until now. In the present work, we demonstrate that this high-T_c hydride phase can be detected by contactless methods, in particular by changes in the surface RF impedance. The RF method reported here, indicates that SC in the La-H system under pressure may occur already at temperatures as high as 267 to 279 K [26, 51].

2.3 | X-Ray Diffraction of the Synthesized Lanthanum Superhydrides

Diffraction of synchrotron radiation is an effective technique for elucidating the structure of polyhydrides under high pressure. The structures of the lanthanum superhydrides in the DACs N1, N2, and N3 were studied using powder X-ray diffraction (XRD), presented in Figure 2). In the case of DAC N1, our XRD analysis shows the formation of a new crystal modification of LaH_{12} at 165 GPa, most likely with a hexagonal symmetry (e.g., $P6_3/mmc$, Figure 2a). In general, an interpretation of the XRD data of the sample in DAC N1 at 165 GPa is challenging. The resulting pattern differs from all the previously experimentally studied ones for the La-H system, but has many similarities with the recently discovered $(La,Ce)H_{12}$ [24]. In terms of volume, the obtained compound approaches the one of LaH_{12} [2]. Although this powder pattern also allows for rhombohedral solutions (e.g., $R\bar{3}m$), we will use the *hP* notation due to the analogy with the theoretically proposed $P6_4$-ScH_{12} [66].

Although the $P6_3/mmc$ structure, with the lattice parameters a = 4.805 Å and c = 3.773 Å, and a unit-cell volume of V = 37.71 Å^3/La, describes the observed diffraction pattern quite well (Figure 2a–c), it should be noted that a c/a ratio of 0.78 is unusually small for the $P6_3/mmc$ space group. Moreover, the reflections 002 and 201 have unexpectedly high intensities, and the 2-10 reflection is actually a split peak due to superstructural features of LaH_{12} or lattice distortion. Hence, another (lower) space group may also describe the structure of the obtained compound. We set the amount of hydrogen in *hP*-LaH_{12} by analogy with the previously reported simple cubic (sc) $Pm\bar{3}m$-LaH_{12} [2, 69–71] with an accuracy of ± 1 H atom. As observed for many known polyhydrides ($(La,Y)H_{10}$ [72, 73], $CeH_{9\text{-}10}$ [7], $ThH_{9\text{-}10}$ [4], PrH_9 [74], etc.), the hexagonal and cubic crystalline modifications form simultaneously, accompany each other, and in many situations cannot be separated or obtained selectively. The same is observed in the case of LaH_{12}. Taking into account subsequent radio-frequency and NMR measurements, this means that we cannot unambiguously attribute the observed transitions to either the hexagonal or cubic phase of LaH_{12}.

The sample in DAC N3, consisting of two phases, was initially synthesized at a pressure of about 115 GPa from LaH_{3-x} and NH_3BH_3. The first phase detected after the pressure synthesis (115 GPa) was simple cubic ($Pm\bar{3}m$) sc-LaH_{12} (Figure 2d,e), as reported previously [2, 69–71]. Structural models for LaH_{12} were proposed by theoretical groups of Defang Duan [66] as $Pm\bar{3}$-ScH_{12}, $Pm\bar{3}$-MgH_{12}, and rare hexagonal $P6_4$-ScH_{12}, and Feng Peng as $Pm\bar{3}m$-LuH_{12} [75]. According to their DFT calculations, which included anharmonic effects, these compounds are high-temperature and even room-temperature superconductors (T_c > 300 K). In these structures, hydrogen exists in an intermediate state (d_{HH} = 1.1–1.2 Å) between molecular (d_{HH} = 0.7–0.8 Å) and atomic hydrogen (d_{HH} = 1.4–1.6 Å). This intermediate state may have a shallow energy minimum. However, in the harmonic approximation $Pm\bar{3}m$-LaH_{12} is dynamically unstable [66]. The anharmonic case will be the subject of future works.

The second phase, distributed in close proximity to LaH_{12}, is the hexagonal modification *hP*-LaH_{12}, which is the main product of the synthesis in DAC N1. This *hP* phase has almost the same volume as the cubic one (Figure 2f,g). Given that both modifications of LaH_{12} have been virtually unknown previously, we decided to focus on their equation of state and stability at low pressures. Successfully, in both DACs N1 and N3, we were able to reduce the pressure to 20-40 GPa without cracking the diamond anvils, and determine the volume and unit cell parameters (Figure 4c,d). Both synthesized modifications of LaH_{12} generally retain the structure of their La sublattices upon decompression to 40 GPa and below (Figures 2f and 4c,d; Figure S17). We expect that as the pressure decreases, the hydrogen sublattice of these compounds changes significantly and becomes more molecular, which is also reflected in the width of the XRD peaks, especially below 82 GPa (see Figure 4c; Figure S17).

DAC N2, made from BeCu alloy, was loaded with metallic La and NH_3BH_3, and heated via a series of IR laser pulses at 147 GPa at the ID27 station of the ESRF. After the laser heating, the pressure increased to 150 GPa. For this sample, we used diamond anvils with a culet diameter of 100 μm. As will be discussed below, the ^{1}H NMR signal of the sample in DAC N2 is several times smaller compared to the spectral intensity observed for the samples in DACs N1 and N3. This likely is caused by a partial destruction of one of the Lenz lenses, as well as a smaller amount of synthesized superhydrides.

According to the XRD analysis (Figure S13), there are two small regions of ~10 μм inside of DAC N2, containing mainly $I4/mmm$-LaH_4 and $Cmcm$-LaH_3. The first of these compounds is a superconductor with a T_c of about 80 to 90 K [76, 77], while the second one is an analogue of the previously found $Cmcm$-$LaH_{\sim 4}$ [28] with a 2 Å^3/La smaller unit-cell volume. This

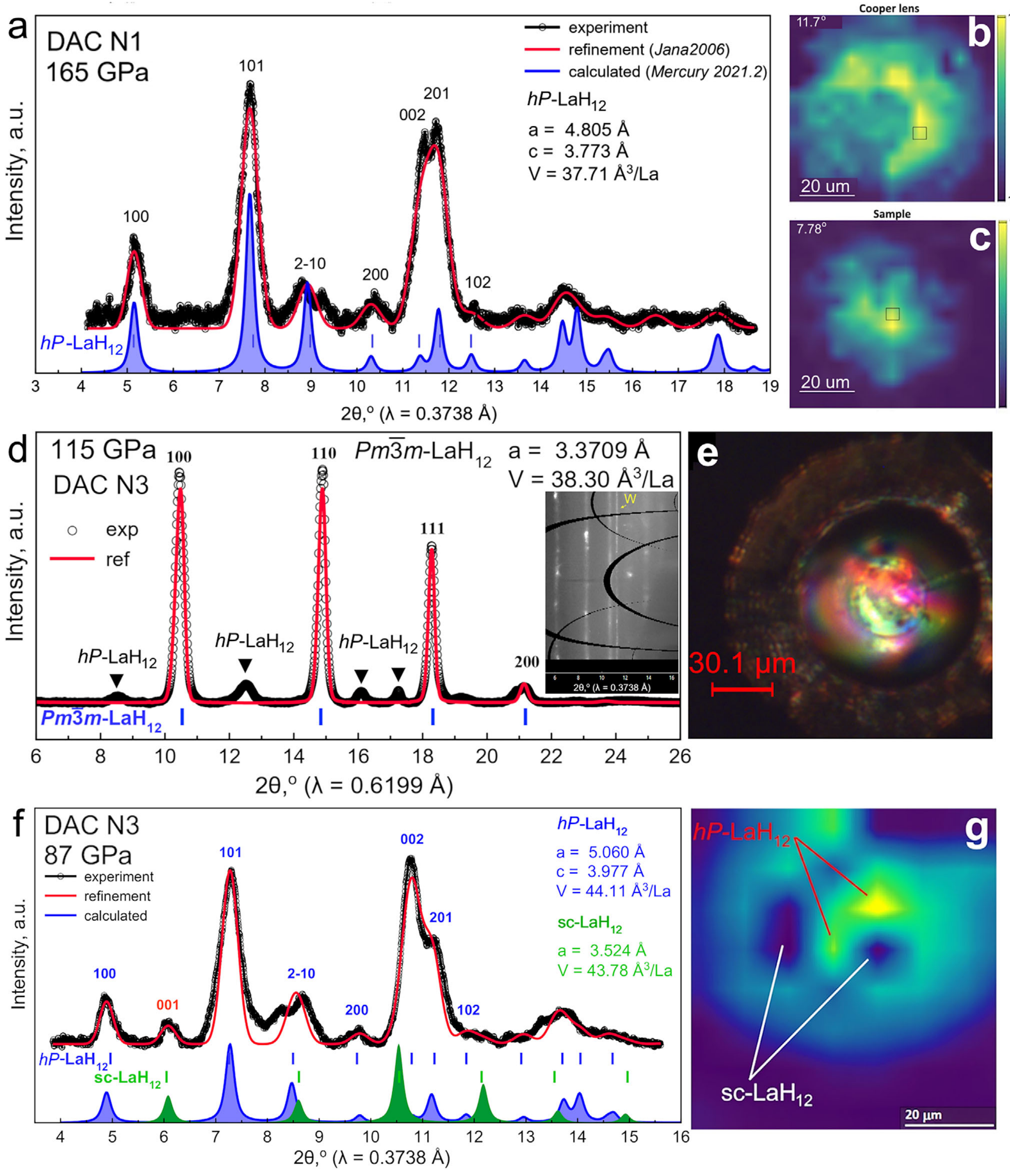

FIGURE 2 | X-ray diffraction studies of the samples in DAC N1 at 165 GPa and in DAC N3 at 87-115 GPa. (a) X-ray diffraction pattern of the sample in DAC N1 and Le Bail refinement of the *hP*-LaH_{12} unit-cell parameters. Black circles are the experimental data, the red line is the Le Bail refinement, and the blue line is the XRD pattern calculated using the Mercury 2021.2 software [67]. For the refinement, we used the $P6_3/mmc$-$LaH_{9\text{-}10}$ structure [56, 57], which reproduces almost all diffraction peaks, but has an unusually small *c/a* ratio of 0.78. The unit-cell volume corresponds to a hydrogen content of about 12 H atoms per La atom. (b) X-ray diffraction mapping of a copper Lenz lens, and (c) the *hP*-LaH_{12} distribution, obtained using the XDI software [68]. The color scale corresponds to the intensity of the strongest XRD reflection for each compound. (d) X-ray diffraction pattern of the sample in DAC N3 and Le Bail refinement of the $Pm\bar{3}m$-LaH_{12} unit-cell parameters. The sample also contains an impurity fraction of hexagonal *hP*-LaH_{12}. Black circles are the experimental data, the red line is the Le Bail refinement. (e) Picture of the DAC N3 culet with the sample. (f) XRD pattern of the sample in DAC N3 after decompression to 87 GPa (see also Figure S17). Black circles are the experimental data, the red line is the Le Bail refinement, and the blue and green filled curves are the XRD patterns of both LaH_{12} modifications, calculated using the Mercury 2021.2 software [67]. (g) X-ray diffraction map of the *hP* (yellow-green) and $Pm\bar{3}m$-LaH_{12} (dark blue) spatial distributions (XDI software [68]).

corresponds to a LaH_3 composition. The T_c of tetragonal LaH_4 was reported to decrease rapidly in an applied magnetic field ($dT_c/dB \approx -2$ K/T [76]). Therefore, T_c should be 66 to 76 K at 7 T. Due to the low content of the superconducting phase and the large spurious background signal with features below 100 K, we cannot confidently state that we have detected the anticipated superconducting transition in LaH_4. However, the disappearance of a series of ^{1}H NMR signals, and a step in the $1/T_1$ vs T dependence around 60 to 70 K may indicate the emergence of SC in LaH_4 (Figure S22).

DAC N4 was loaded with LaH_{3-x} and NH_3BH_3. The material was heated by an IR laser at around 150 GPa, but it broke down in the following days with a pressure drop to below 50 GPa. Due to this, DAC N4 was used only for a narrow set of experiments (Figure S23).

2.4 | Preliminary NMR Experiments

^{1}H NMR experiments on micron-sized samples compressed between diamond anvils are inevitably associated with parasitic hydrogen signals from different parts of the high-pressure DACs, such as the organic adhesive used to glue the diamond anvils to the seats, wire insulation, capacitors, soldering paste, and the printed circuit board (PCB) supporting the excitation coils. Since the laser heating of the starting material in the DACs never leads to a complete decomposition of NH_3BH_3, the study of the residual signal of this compound is important as well. Therefore, before starting the experiments with the polyhydrides in the DACs N1-N4, we investigated several calibration samples at temperatures from 10 to 300 K. We studied the following test samples:

A. An empty DAC with a Lenz-lens system (Figure S8);
B. The same DAC, loaded with a piece of ^{27}Al foil and NH_3BH_3 (Figures S6 and S7);
C. A bulk sample of NH_3BH_3 in a conventional NMR resonator (Figure S9);
D. A piece of PCB, used as support for the Lenz-lens excitation coils (Figure S10).

The examination of the empty DAC with Lenz lenses (test "A") indicates the presence of some volatile H-containing impurities in the DAC: The NMR signal intensity significantly decreases with time. The low intensity of the ^{1}H NMR signal of the empty DAC prevents a T_1 measurement (Figure S8).

As a result of the preparatory experiment "B", we found that the Lenz-lens system does indeed allow a reliable detection of the ^{27}Al NMR signal from a small piece of Al foil from the DAC sample volume. The spin-lattice relaxation curve $I(\tau)$ and the stretching exponent indicate a non-uniform distribution of the RF field in the sample (Figure S6), which in this case is due to a non-ideal geometry of the Lenz lenses in the non-pressurized DAC.

The ^{1}H signal intensity was found to sufficiently strong when we placed a micron-sized sample of NH_3BH_3 together with the ^{27}Al foil in the chamber of the test DAC "B" (Figures S6 and S7). Besides the presence of a kink in the temperature dependence of the integral intensity $I(T)$ around 250 K, the nuclear spin-lattice relaxation rate $1/T_1T$ yields no particular features between 50 and 300 K, which is important to note for the subsequent experiments on the lanthanum hydrides.

The ^{1}H NMR experiments on a bulk sample of NH_3BH_3 (test "C") yield a rather complex, two-component T_1 relaxation. For instance, $1/T_1T$ shows a rise below 210 K, with a maximum at 100 to 150 K (Figure S9). This is possibly related to low-temperature phase transitions in NH_3BH_3, as reported previously (see also Ref [78]).

Finally, the teflon PCB (test "D") gives an insignificant ^{1}H NMR signal without pronounced features above 170 K (Figure S10). Thus, by performing these preliminary experiments, we have verified that the ^{1}H NMR signal discussed below indeed dominantly stems from the samples of compressed lanthanum polyhydrides.

2.5 | ^{1}H NMR of Lanthanum Superhydrides at Pressures up to 165 GPa

We used a system of Lenz lenses (Figure 3a,b), deposited on diamond anvils, to perform NMR measurements of micron-sized samples under pressure. Our ^{1}H NMR study, using DAC N1 in a magnetic field of 7 T (ν_0 = 298 MHz), employing a conventional spin-echo pulse sequence, was carried out during cooling between 300 and 10 K (Figure 3c). At high temperatures, the spectrum can be described as a composition of at least four peaks ("a–d", Figure 3d), three of which ("a–c") disappear below 230 K and yield a negative frequency shift with decreasing temperature ($d\nu/dT > 0$). These peaks are attributed to different lanthanum superhydrides that form at 165 GPa, when the La/ NH_3BH_3 mixture is heated [2, 28, 59]. As the XRD analysis demonstrated (Figure 2), the main phase synthesized in DAC N1 is hexagonal hP-LaH_{12}. The very narrow peak "d" disappears below 200 K with $d\nu/dT < 0$.

Between 300 K and T_c^{onset} = 260 K, we find a linear decrease of the integral intensity of the ^{1}H NMR spectrum, as well as a pronounced slope change at T_c^{onset} (Figure 3e). Below T_c^{onset}, our data show a strong suppression of the NMR intensity, which saturates at 211 K. Between T_c^{onset} and 220 K, we observe pronounced changes in all spectral characteristics, i.e., the frequency shift, spectral width, and area ("intensity") of the ^{1}H NMR spectrum (Figure 3d–f). The residual, broad low-temperature ^{1}H NMR spectrum stems from the background of non-superconducting hydrogen-containing compounds, residual NH_3BH_3, products of its thermal decomposition, and lower La hydrides (Figure 3c,d). We note that, although these background signals may partially contribute to the change in spectral characteristics in the superconducting transition region, this does not affect the qualitative behavior in the detection of the superconducting transition by means of NMR. At 165 GPa and 7 T, the observed $T_c^{50\%}$ is (227 ± 5) K (Figure 3f). This temperature corresponds to the SC transition in the best-known lanthanum superhydrides in a field of 7 T, determined via electrical-transport measurements at the middle of the resistance drop ($R_{50\%}$ criterion, see Ref [2].). At 4 T, the superconducting transition of the lanthanum superhydride in

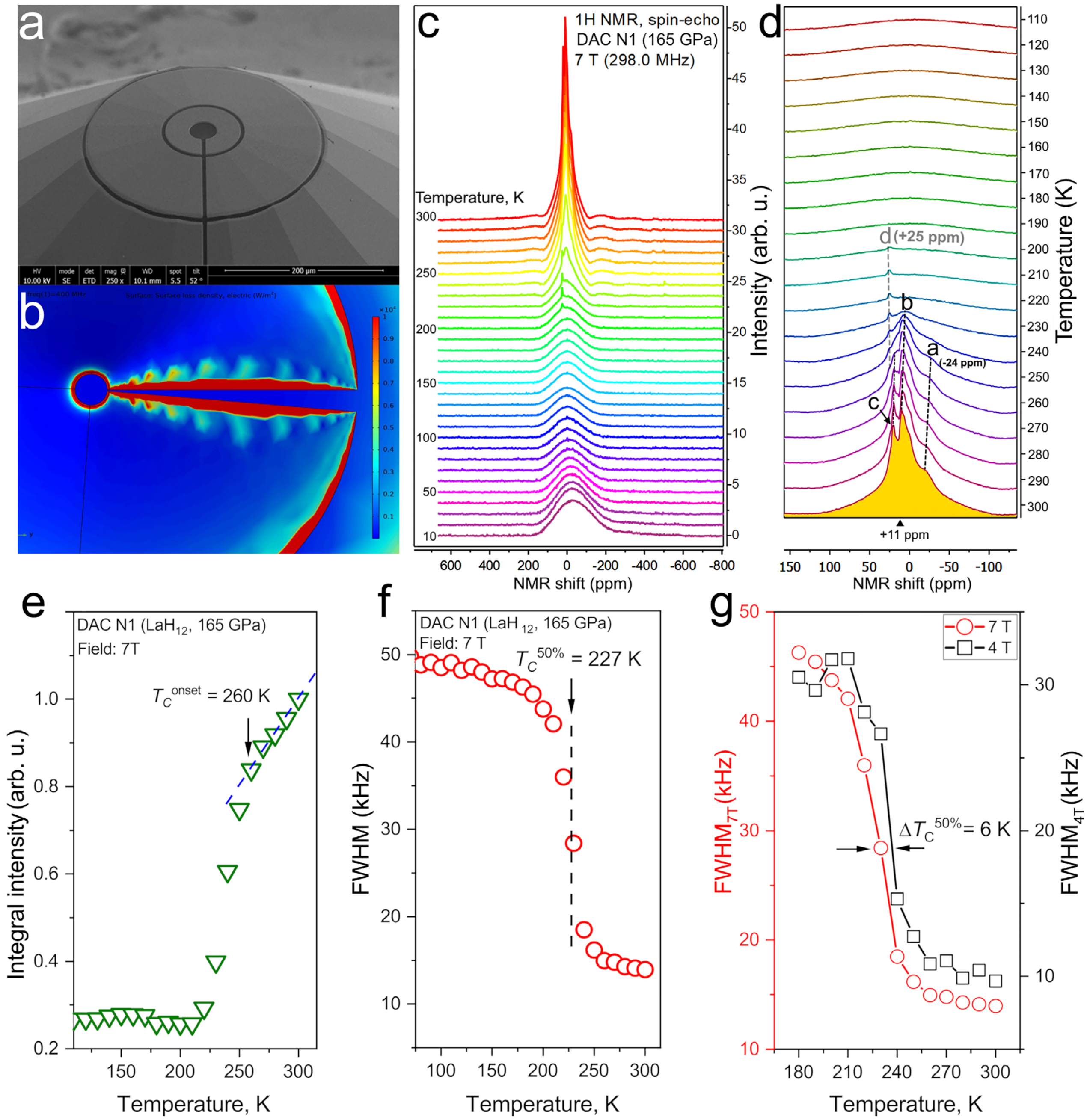

FIGURE 3 | ^{1}H Nuclear magnetic resonance experiments using DAC N1. (a) Scanning electron microscopy of the copper Lenz lens of DAC N1, prepared by using a focused Ga-ion beam. (b) Modeling of the distribution of surface current density losses (in W/m^2) in the Lenz lens at 400 MHz (using COMSOL Multiphysics [79]). (c) Stack of ^{1}H NMR spectra, recorded during cooling from 300 to 10 K in steps of 10 K. (d) ^{1}H NMR spectra in the temperature regime of the superconducting transition. The structure of the signal above 240 K is composed of at least four different peaks ("a–d"). (e) Temperature dependence of the ^{1}H NMR signal area ("intensity") between 115 and 300 K. T_c^{onset} = 260 K denotes the onset of the pronounced intensity decrease. (f) Temperature dependence of the ^{1}H NMR linewidth (FWHM = full width at half maximum) between 75 and 300 K, yielding $T_c(50\,\%) = (227 \pm 5)$ K. (g) Temperature dependence of FWHM for applied magnetic fields of 4 and 7 T. At 4 T, T_c is approximately 6 K higher.

DAC N1 is shifted higher in temperature, to $T_c^{50\%} = (235 \pm 5)$ K (Figure 3g). The offset T_c also increases from 211 K (7 T) to 220 K (4 T), see Figure S19.

To confirm the onset of SC as an origin of the pronounced change in the spectral features of the sample in DAC N1 and to probe the electronic low-energy excitations, we also measured the nuclear spin-lattice relaxation time T_1. The relaxation rate $1/T_1T$ of the samples in DACs N1 and N3 begins to decrease at temperatures above 260 K at 7 T (Figure 4a). A sharp drop in $1/T_1T$ by 3-6 times in the temperature range between 220 and 260 K, not observed in the calibration samples and other DACs, indicates the superconducting nature of the transition in the lanthanum-hydride samples in DACs N1 and N3. This confirms our findings based on the RF transmission studies discussed above (Figure 1).

For the DACs N1 and N3, the overall behavior of the ^{1}H NMR spectra and the spin-lattice relaxation time is very similar. This

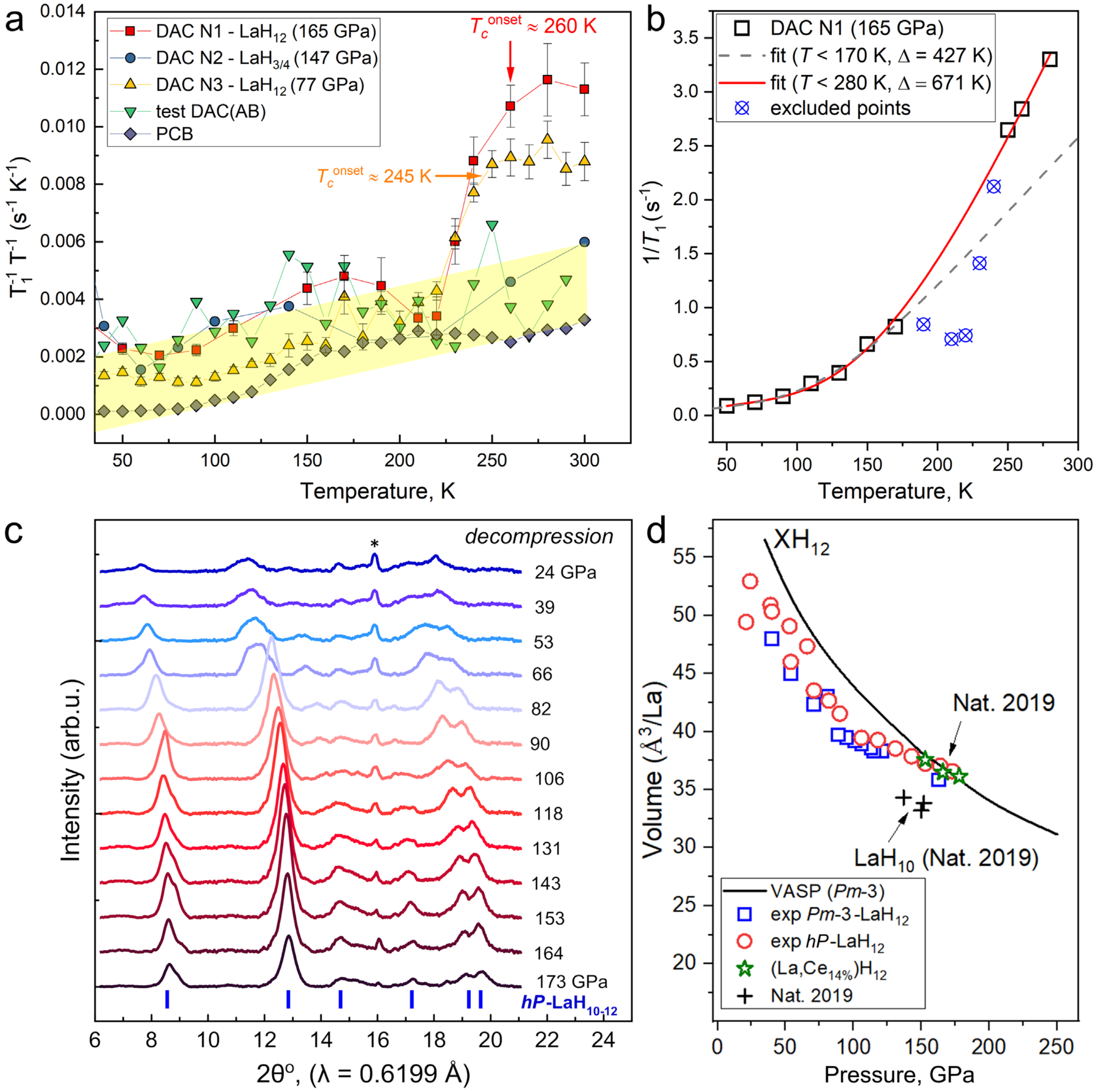

FIGURE 4 | ^{1}H nuclear spin-lattice relaxation rate $(T_1T)^{-1}$ and the equation of state of LaH_{12}. (a) Temperature dependence of the relaxation rate $1/T_1T$. There is a pronounced drop in the relaxation rate of the samples in DACs N1 and N3 below 260 and 245 K, respectively. This is associated with the presence of the LaH_{12} phase, which is absent in the other DACs and test samples. (b) Fits using $1/T_1 = Ae^{-\Delta/T} + CT$ (here we set $k_B = 1$) to describe the temperature-dependent $1/T_1$ of the sample in DAC N1 at 165 GPa and 7 T. Here, A and C are fit parameters, as well as the superconducting gap $\Delta = \Delta(0)$. We performed fits for temperatures below 170 and 280 K, indicated by a gray dashed line and a red solid line, respectively. (c) Stack of integrated XRD patterns obtained during decompression of the DAC N1 with hexagonal LaH_{12} from 173 GPa to 24 GPa at room temperature. (d) Equation of state $V(P)$ of cubic ($Pm\bar{3}m$) and hexagonal (hP) LaH_{12} compared with the theoretical calculations (black line) and data from Ref. [2] ("Nat. 2019"). [Correction added on 12 February 2026, after first online publication: Figure 4d is updated.]

can be understood by the presence of the same hP-LaH_{12} phase in both DACs (Figure 2).

Decompression of DACs N1 and N3 revealed that La-sublattices in both phase modifications of LaH_{12} are very stable and decompose only at pressures about 20–40 GPa (Figure 4d; Figure S17). The hexagonal modification of LaH_{12} undergoes a sharp structural distortion with broadening of the diffraction peaks between 82 and 66 GPa. A comparison of the calculated equation of state $V(P)$ and the experimental data (Figure 4d) also suggests that, when the pressure decreases below 140–150 GPa, the stoichiometry of the compounds may be lower than in XH_{12} and should be written as LaH_{12-x} (x = 0…1).

3 | Discussion

The complete volume displacement of an applied external magnetic field in the superconducting state is a key characteristic of type-I superconductors. By contrast, in type-II superconductors, in particular for granulated ones [25], the field penetrates the sample volume [80–82]. As the NMR signal intensity is proportional to the penetrated sample volume, this facilitates NMR measurements even at temperatures below T_c (Figure 4a,b). The measured spin-lattice relaxation time of the sample in DAC N1 at 300 K is about 300 ms, and the product is $TT_1 \approx 88$ sK. Comparing the low-temperature behavior of the spin-lattice relaxation of the samples in DACs N1 and N2, we note that the differences in TT_1 are small: $TT_1 = 573$ sK at 50 K for the sample in DAC N1, and 340 sK at 40 K for the sample in DAC N2. This is not surprising, given the fact that superconducting phases yield only a very small contribution to the NMR signal at $T << T_c$. The ^{1}H signal at low temperatures is mainly due to the residual non-superconducting hydrogen-containing compounds.

As Figures 4a,b, and S20 show, there is a region of increased spin-lattice relaxation rate between about 100 and 227 K for the sample in DAC N1, which can be associated with either LaH_{12} or residual NH_3BH_3. Phenomenologically, this feature in $1/T_1$ vs T resembles the relaxation behavior of ^{27}Al NMR measurements, studied in the classical Hebel-Slichter [38, 39] and Redfield-Anderson [37] experiments (Figure S21). In this scenario, the hump below $T_c^{50\%}$ for the sample in DAC N1 may be caused by the contribution of a Hebel-Slichter-type coherence peak, indicating the opening of the SC gap and the appearance of narrow maxima in the density of quasiparticle states $N(E)$. Since the dependence $1/T_1 \propto N(E)^2$ is quadratic, the presence of a maximum in $N(E)$ leads to a peak in $1/T_1$ (the Hebel-Slichter peak). If this increase of the relaxation rate is indeed related to such a coherence peak and not to a residual amount of NH_3BH_3 (Figure S9), it would be a strong argument in favor of conventional electron-phonon pairing in lanthanum superhydrides [83, 84].

However, we would like to emphasize another observation, based on our T_1 data. In many superconductors, antiferromagnetic fluctuations [85], as well as a strong electron-phonon interaction [86], may suppress a possible Hebel-Slichter peak. LaH_{12} is expected to be a superconductor in the strong-coupling limit. Indeed, describing the temperature dependence of $1/T_1$ below T_c using an exponential fit allows to determine the superconducting gap of LaH_{12} at 165 GPa. As shown in Figure 4b (and Figure S20), such fits to the $1/T_1$ data for different temperature regimes provide an estimate of the superconducting gap $\Delta(0)$. We obtain values between about 427 and 671 K (36.8 and 57.8 meV), yielding $R_\Delta = 2\Delta(0)/k_B T_c$ of about 3.76 to 5.16, in qualitative agreement with the strong electron-phonon coupling extension of the BCS theory proposed by Migdal and Eliashberg [87, 88].

The onset temperature of the probable superconducting transition in LaH_{12} deserves a separate discussion. Although even in pure $Fm\bar{3}m$-LaH_{10} in zero field, the critical temperature T_c^{onset} does not exceed about 250 K, in our experiment, we observe an unusual behavior of the NMR spectra and $1/T_1T$ right above 260 K at 7 T. Considering a typical value of the derivative $dB_{c2}/dT \approx -1$ T/K for superhydrides [89, 90], we estimate that at zero field, SC in the sample in DAC N1 sets in already around 267 K, which is significantly higher than the T_c^{onset} observed in electrical-transport measurements of LaH_{10} [2]. Thus, the results of our NMR study in magnetic fields of 4 and 7 T agree well with the RF transmission measurements in zero field (Figure 1).

Measurements of the electrical transport are limited to the current path of least resistance. By contrast, RF methods sense the full bulk of the sample. Hence, differences in T_c^{onset} detected by these techniques are a natural consequence. Once SC sets in, the resistance drops to zero and any information below that transition is hidden. In inhomogeneous granular superconductors consisting of multiple phases with varying T_c, a series-connected normal-metallic and superconducting resistance may be sensed. Hence, step-like transitions with non-zero resistances may be detected. Indeed, such features have been noted previously in La-H [3, 50, 65] and La-Sc-H systems [26, 91] at temperatures much higher than 250 K. It is interesting to note that similar anomalies were also observed in the high-frequency AC-susceptibility measurements on $LaH_{10\pm x}$ samples [51]. Although the aim of this work is not to provide a definitive proof of a near-room temperature superconductivity in LaH_{12}, but rather to demonstrate the feasibility of contactless research methods, ^{1}H NMR and RF transmission, the data we obtained indicate the prospects for continuing the study of this exotic lanthanum polyhydride.

4 | Conclusions

Employing ^{1}H nuclear magnetic resonance spectroscopy and radio-frequency transmission measurements, we studied five lanthanum-hydride samples, including two crystal modifications of LaH_{12}, LaH_{9+x}, tetragonal LaH_4, and LaH_3, at various pressures from 19 to 165 GPa in magnetic fields of 0, 4, and 7 T. The transition in the newly discovered LaH_{12} is characterized by a strong suppression of the ^{1}H-NMR signal intensity below about 260 K in a magnetic field of 7 T and may have a superconducting nature. Furthermore, it is accompanied by a pronounced change in all NMR characteristics, including the spin-lattice relaxation rate $1/T_1T$, which exponentially decreases at temperatures below T_c. Our estimate of the superconducting gap in LaH_{12} gives $\Delta(0)$ of about 427 to 671 K (corresponding to 36.8 to 57.8 meV) and $R_\Delta = 2\Delta(0)/k_B T_c$ of about 3.76 to 5.16, in accordance with the strong-coupling scenario in lanthanum superhydrides.

We confirmed these observations by additional radio-frequency transmission experiments on the same samples using a transformer configuration, where Lenz lenses act as primary and secondary coils. The transmission amplitude exhibits abrupt changes, already setting in at 267 ± 5 K (in zero field). Remarkably, the La-H system contains phases with significantly higher T_c than what was previously reported based on electrical-transport measurements. In the two samples in DACs N1 and N3, the detected changes in the ^{1}H-NMR spectral characteristics, and, most importantly, the spin-lattice relaxation rate $1/T_1T$, start about 15-20 K above the zero-field onset T_c of the canonical LaH_{10}, determined by means of electrical-transport measurements.

Author Contributions

D.V.S., D.Z., and I.A.T. designed the experiments, prepared the DACs including sputtering of Lenz lenses and synthesis of the lanthanum hydride samples, did the COMSOL modelling, performed the RF transmission measurements, transport, powder X-ray diffraction studies, and analyzed the XRD data. F.B., D.V.S., D.Z., and S.L. performed the NMR measurements and analyzed the NMR data. J.W., H.K., and T.H. supervised the work at HZDR. V.V.S. supervised the work at HPSTAR. All authors contributed to the discussion of the results and the preparation of the manuscript.

Acknowledgements

D.V.S. and D.Z. thank the National Natural Science Foundation of China (NSFC, Grant No. 12350410354) and the Beijing Natural Science Foundation (Grant No. IS23017) for the support of this research. D.Z. thanks the China Postdoctoral Science Foundation (No. 2023M740204) and Fundamental Research Funds from HPSTAR for support of this research. D.S. and D.Z. are grateful for financial support from the EMFL-ISABEL project. This work was supported by the National Key Research and Development Program of China (Grant 2023YFA1608900, subproject 2023YFA1608903). V.V.S. acknowledges financial support from the Shanghai Science and Technology Committee, China (No. 22JC1410300) and Shanghai Key Laboratory of Materials Frontier Research in Extreme Environments (MFree), China (No. 22dz2260800). I.A.T. acknowledges the support by the state assignment of the Kurchatov Complex of Crystallography and Photonics (KKKiF). The authors express our gratitude to Dr. Fuyang Liu, Dr. Yanping Yang, and Dr. Hongliang Dong from Beijing and Shanghai HPSTAR for their help with the Ga FIB ion etching and magnetron sputtering of Al_2O_3, respectively. The authors also thank Dr. Thomas Meier (HPSTAR, Beijing) for technical support and drawing our attention to the NMR research using diamond anvil cells. The authors thank Prof. Yang Ding's group, especially Dr. Jianbo Zhang, at HPSTAR, Beijing, for allowing us to use the Raman spectrometer and the magnetron sputtering system. The authors would like to express our gratitude to Dr. Liuxiang Yang (HPSTAR, Beijing) for the laser heating of our samples. The authors thank Dr. Xiaoli Huang (Jilin University) and Dr. Liling Sun (HPSTAR, Beijing) for assistance with X-ray diffraction studies at the Shanghai synchrotron research facility. The authors also express our gratitude to the teams of the high-pressure stations ID27 (ESRF) and BL15U1 (SSRF) for their help in the XRD investigations. The authors acknowledge support from the Deutsche Forschungsgemeinschaft (DFG) through the Würzburg-Dresden Cluster of Excellence on Complexity, Topology and Dynamics in Quantum Matter—ctd.qmat (EXC 2147, Project No. 390858490), as well as the support of the HLD at HZDR, a member of the European Magnetic Field Laboratory (EMFL). The authors thank the Department for Physics of Quantum Materials at the MPI CPfS (Dresden, Germany) and Ion Beam Center at HZDR (Dresden, Germany) for putting their FIB infrastructure at our disposal.

Ethical Statement

There are no human subjects in this article and informed consent is not applicable.

Conflicts of Interest

The authors declare no conflicts of interest.

Data Availability Statement

The data that support the findings of this study are available from the corresponding author upon reasonable request.

References

1. A. P. Drozdov, M. I. Eremets, I. A. Troyan, V. Ksenofontov, and S. I. Shylin, "Conventional Superconductivity at 203 Kelvin at High Pressures in the Sulfur Hydride System," *Nature* 525 (2015): 73–76, https://doi.org/10.1038/nature14964.

2. A. P. Drozdov, P. P. Kong, V. S. Minkov, et al., "Superconductivity at 250 K in Lanthanum Hydride Under High Pressures," *Nature* 569 (2019): 528–531, https://doi.org/10.1038/s41586-019-1201-8.

3. M. Somayazulu, M. Ahart, A. K. Mishra, et al., "Evidence for Superconductivity Above 260 K in Lanthanum Superhydride at Megabar Pressures," *Physical Review Letters* 122 (2019): 027001, https://doi.org/10.1103/PhysRevLett.122.027001.

4. D. V. Semenok, A. G. Kvashnin, A. G. Ivanova, et al., "Superconductivity at 161 K in Thorium Hydride ThH_{10}: Synthesis and Properties," *Materials Today* 33 (2020): 36–44.

5. P. Kong, V. S. Minkov, M. A. Kuzovnikov, et al., "Superconductivity up to 243 K in the Yttrium-Hydrogen System Under High Pressure," *Nature Communications* 12 (2021): 5075, https://doi.org/10.1038/s41467-021-25372-2.

6. I. A. Troyan, D. V. Semenok, A. G. Kvashnin, et al., "Anomalous High-Temperature Superconductivity in YH 6," *Advanced Materials* 33 (2021): 2006832, https://doi.org/10.1002/adma.202006832.

7. W. Chen, D. V. Semenok, X. Huang, et al., "High-Temperature Superconducting Phases in Cerium Superhydride with a T_c up to 115 K Below a Pressure of 1 Megabar," *Physical Review Letters* 127 (2021): 117001, https://doi.org/10.1103/PhysRevLett.127.117001.

8. I. A. Troyan, D. V. Semenok, A. G. Ivanova, et al., "High-Temperature Superconductivity in Hydrides," *Physics-Uspekhi* 65 (2022): 748–761, https://doi.org/10.3367/UFNe.2021.05.039187.

9. D. Semenok, Computational Design of New Superconducting Materials and Their Targeted Experimental Synthesis (PhD Thesis, Skolkovo Institute of Science and Technology, 2022).

10. N. W. Ashcroft, "Hydrogen Dominant Metallic Alloys: High Temperature Superconductors?," *Physical Review Letters* 92 (2004): 187002, https://doi.org/10.1103/PhysRevLett.92.187002.

11. F. Peng, Y. Sun, C. J. Pickard, R. J. Needs, Q. Wu, and Y. Ma, "Hydrogen Clathrate Structures in Rare Earth Hydrides at High Pressures: Possible Route to Room-Temperature Superconductivity," *Physical Review Letters* 119 (2017): 107001, https://doi.org/10.1103/PhysRevLett.119.107001.

12. H. Liu, I. I. Naumov, R. Hoffmann, N. W. Ashcroft, and R. J. Hemley, "Potential High-T_c Superconducting Lanthanum and Yttrium Hydrides at High Pressure," *Proceeding of the National Academy of Sciences* 114 (2017): 6990–6995.

13. D. Duan, Y. Liu, F. Tian, et al., "Pressure-Induced Metallization of Dense $(H_2S)_2H_2$ with High-T_c Superconductivity," *Scientific Reports* 4 (2014): 6968, https://doi.org/10.1038/srep06968.

14. P. Giannozzi, S. Baroni, N. Bonini, et al., "QUANTUM ESPRESSO: A Modular and Open-Source Software Project for Quantum Simulations of Materials," *Journal of Physics-Condensed Matter* 21 (2009): 395502.

15. S. Baroni, S. D. Gironcoli, A. D. Corso, and P. Giannozzi, "Phonons and Related Crystal Properties from Density-Functional Perturbation Theory," *Reviews of Modern Physics* 73 (2001): 515–562, https://doi.org/10.1103/RevModPhys.73.515.

16. G. Kresse and J. Furthmüller, "Efficient Iterative Schemes for Ab Initio Total-Energy Calculations Using a Plane-Wave Basis Set," *Physical Review B* 54 (1996): 11169–11186, https://doi.org/10.1103/PhysRevB.54.11169.

17. C. W. Glass, A. R. Oganov, and N. Hansen, "USPEX—Evolutionary Crystal Structure Prediction," *Computer Physics Communications* 175 (2006): 713–720, https://doi.org/10.1016/j.cpc.2006.07.020.

18. A. R. Oganov and C. W. Glass, "Crystal Structure Prediction Using *Ab Initio* Evolutionary Techniques: Principles and Applications," *Journal of Chemical Physics* 124 (2006): 244704, https://doi.org/10.1063/1.2210932.

19. Y. Wang, J. Lv, L. Zhu, and Y. Ma, "Crystal Structure Prediction via Particle-Swarm Optimization," *Physical Review B* 82 (2010): 094116, https://doi.org/10.1103/PhysRevB.82.094116.

20. C. J. Pickard and R. J. Needs, "Ab Initio Random Structure Searching," *Journal of Physics-Condensed Matter* 23 (2011): 053201.

21. M. Lüders, M. A. L. Marques, N. N. Lathiotakis, et al., "Ab Initio Theory of Superconductivity. I. Density Functional Formalism and Approximate Functionals," *Physical Review B* 72 (2005): 024545.

22. M. A. L. Marques, M. Lüders, N. N. Lathiotakis, et al., "*Ab Initio* Theory of Superconductivity. II. Application to Elemental Metals," *Physical Review B* 72 (2005): 024546, https://doi.org/10.1103/PhysRevB.72.024546.

23. I. Errea, M. Calandra, and F. Mauri, "Anharmonic Free Energies and Phonon Dispersions from the Stochastic Self-Consistent Harmonic Approximation: Application to Platinum and Palladium Hydrides," *Physical Review B* 89 (2014): 064302, https://doi.org/10.1103/PhysRevB.89.064302.

24. D. V. Semenok, I. A. Troyan, D. Zhou, W. Chen, H.-K. Mao, and V. V. Struzhkin, "Observation of the Josephson Effect in Superhydrides: DC SQUID Based on $(La,Ce)H_{10+x}$ with Operating Temperature of 179 K," *The Innovation Materials* 3 (2025): 100115, https://doi.org/10.59717/j.xinn-mater.2024.100115.

25. D. V. Semenok, A. V. Sadakov, D. Zhou, et al., "Superconducting Memory and Trapped Magnetic Flux in Ternary Lanthanum Polyhydrides," *Materials Today Physics* 49 (2024): 101595, https://doi.org/10.1016/j.mtphys.2024.101595.

26. D. V. Semenok, A. V. Sadakov, D. Zhou, O. A. Sobolevskiy, S. Luther, T. Helm, V. M. Pudalov, I. A. Troyan, and V. V. Struzhkin, Superconducting memory and trapped magnetic flux in ternary lanthanum polyhydrides. Materials Today Physics (2024). 49, 101595, https://doi.org/10.1016/j.mtphys.2024.101595.

27. A. Aslandukova, A. Aslandukov, D. Laniel, et al., "Diverse High-Pressure Chemistry in $Y\text{-}NH_3BH_3$ and Y–Paraffin Oil Systems," *Science Advances* 10 (2024): adl5416, https://doi.org/10.1126/sciadv.adl5416.

28. D. Laniel, F. Trybel, B. Winkler, et al., "High-Pressure Synthesis of Seven Lanthanum Hydrides with a Significant Variability of Hydrogen Content," *Nature Communications* 13 (2022): 6987, https://doi.org/10.1038/s41467-022-34755-y.

29. D. V. Semenok, B. L. Altshuler, and E. A. Yuzbashyan, "Fundamental Limits on the Electron-Phonon Coupling and Superconducting T_c," *Adv. Mater*. 37, no. 40 (2025): 2507013, https://doi.org/10.1002/adma.202507013.

30. T. Sakakibara, T. Goto, and N. Miura, "Contactless Transport Measurement of Metals in Pulsed High Magnetic Fields," *Review of Scientific Instruments* 60 (1989): 444–449, https://doi.org/10.1063/1.1140398.

31. Y. A. Timofeev, V. V. Struzhkin, R. J. Hemley, H.-K. Mao, and E. A. Gregoryanz, "Improved Techniques for Measurement of Superconductivity in Diamond Anvil Cells by Magnetic Susceptibility," *Review of Scientific Instruments* 73 (2002): 371–377, https://doi.org/10.1063/1.1431257.

32. T. Meier, A. Aslandukova, F. Trybel, et al., "In Situ High-Pressure Nuclear Magnetic Resonance Crystallography in One and Two Dimensions," *Matter and Radiation at Extremes* 6 (2021): 068402.

33. H. Günther, *NMR Spectroscopy: Basic Principles, Concepts and Applications in Chemistry*, 3rd ed. (John Wiley & Sons, 2013).

34. I. I. Rabi, J. R. Zacharias, S. Millman, and P. Kusch, "A New Method of Measuring Nuclear Magnetic Moment," *Physical Review* 53 (1938): 318, https://doi.org/10.1103/PhysRev.53.318.

35. K. Müller and M. Geppi, *Solid State NMR: Principles, Methods, and Applications* (John Wiley & Sons, 2021).

36. L. N. Cooper, "Microscopic Quantum Interference Effects in the Theory of Superconductivity," *Science* 181, no. 4103 (1972): 908–916.

37. A. G. Anderson and A. G. Redfield, "Nuclear Spin-Lattice Relaxation in Metals," *Physical Review* 116 (1959): 583–591, https://doi.org/10.1103/PhysRev.116.583.

38. L. C. Hebel and C. P. Slichter, "Nuclear Relaxation in Superconducting Aluminum," *Physical Review* 107 (1957): 901–902, https://doi.org/10.1103/PhysRev.107.901.

39. L. C. Hebel and C. P. Slichter, "Nuclear Spin Relaxation in Normal and Superconducting Aluminum," *Physical Review* 113 (1959): 1504–1519, https://doi.org/10.1103/PhysRev.113.1504.

40. W. D. Knight, "Nuclear Magnetic Resonance Shift in Metals," *Physical Review* 76 (1949): 1259–1260, https://doi.org/10.1103/PhysRev.76.1259.2.

41. D. F. Smith and C. P. Slichter, "The Study of Mechanisms of Superconductivity by NMR Relaxation," *Lecture Notes in Physics* 684 (2006): 243–295.

42. J. Korringa, "Nuclear Magnetic Relaxation and Resonnance Line Shift in Metals," *Physica* 16 (1950): 601–610, https://doi.org/10.1016/0031-8914(50)90105-4.

43. T. Meier, N. Wang, D. Mager, J. G. Korvink, S. Petitgirard, and L. Dubrovinsky, "Magnetic Flux Tailoring Through Lenz Lenses for Ultrasmall Samples: A New Pathway to High-Pressure Nuclear Magnetic Resonance," *Science Advances* 3 (2017): aao5242, https://doi.org/10.1126/sciadv.aao5242.

44. Y. Fu, R. Tao, L. Zhang, et al., "Trace Element Detection in Anhydrous Minerals by Micro-Scale Quantitative Nuclear Magnetic Resonance Spectroscopy," *Nature Communications* 15 (2024): 7293, https://doi.org/10.1038/s41467-024-51131-0.

45. T. Meier, F. Trybel, S. Khandarkhaeva, et al., "Pressure-Induced Hydrogen-Hydrogen Interaction in Metallic FeH Revealed by NMR," *Physical Review X* 9 (2019): 031008.

46. T. Meier, D. Laniel, and F. Trybel, "Direct Hydrogen Quantification in High-Pressure Metal Hydrides Matter and Radiation at Extremes Direct Hydrogen Quantification in High-Pressure Metal Hydrides," *Matter and Radiation at Extremes* 8 (2023): 18401.

47. T. Meier, F. Trybel, G. Criniti, et al., "Proton Mobility in Metallic Copper Hydride from High-Pressure Nuclear Magnetic Resonance," *Physical Review B* 102 (2020): 165109, https://doi.org/10.1103/PhysRevB.102.165109.

48. T. Meier, D. Laniel, M. Pena-Alvarez, et al., "Nuclear Spin Coupling Crossover in Dense Molecular Hydrogen," *Nature Communications* 11 (2020): 6334, https://doi.org/10.1038/s41467-020-19927-y.

49. M. Yang, Y. Zhou, R. Jana, T. Nakagawa, Y. Fu, and T. Meier, "Hexagonal to Monoclinic Phase Transition in Dense Hydrogen Phase III Detected by High-Pressure NMR," *arXiv* (2024): 240719368.

50. T. Shitaokoshi, S. Kawachi, T. Nomura, F. F. Balakirev, and Y. Kohama, "Radio Frequency Electrical Resistance Measurement Under Destructive Pulsed Magnetic Fields," *Review of Scientific Instruments* 94 (2023): 094706.

51. N. Spengler, P. T. While, M. V. Meissner, U. Wallrabe, and J. G. Korvink, "Magnetic Lenz Lenses Improve the Limit-of-Detection in Nuclear Magnetic Resonance," *PLoS ONE* 12 (2017): 0182779, https://doi.org/10.1371/journal.pone.0182779.

52. D. Sun, V. S. Minkov, S. Mozaffari, et al., "High-Temperature Superconductivity on the Verge of a Structural Instability in Lanthanum Superhydride," *Nature Communications* 12 (2021): 6863, https://doi.org/10.1038/s41467-021-26706-w.

53. A. P. Drozdov, V. S. Minkov, S. P. Besedin, et al., "Superconductivity at 215K in Lanthanum Hydride at High Pressures," *arXiv* (2018): 180807039.

54. Y. Chen, J. Wen, Z.-X. He, et al., "Imaging Magnetic Flux Trapping in Lanthanum Hydride Using Diamond Quantum Sensors," *arXiv* (2025): 251021877.

55. P. Dalladay-Simpson, G. Marchese, Z.-Y. Cao, et al., "Evidence for a New Phase of Dense Hydrogen Above 325 Gigapascals," *Nature* 529, no. 7584 (2025): 63–77.

56. I. Errea, F. Belli, L. Monacelli, et al., "Quantum Crystal Structure in the 250-Kelvin Superconducting Lanthanum Hydride," *Nature* 578 (2020): 66–69, https://doi.org/10.1038/s41586-020-1955-z.

57. I. A. Kruglov, D. V. Semenok, H. Song, et al., "Superconductivity of LaH_{10} and LaH_{16} Polyhydrides," *Physical Review B* 101 (2020): 024508, https://doi.org/10.1103/PhysRevB.101.024508.

58. D. V. Semenok, D. Zhou, J. Zhang, et al., "Radio-Frequency Method for Detecting Superconductivity Under High Pressure," *arXiv* (2025): 250900563.

59. D. Semenok, I. Troyan, D. Zhou, et al., "Ternary Superhydrides Under Pressure of Anderson's Theorem: Near-Record Superconductivity in $(La,Sc)H_{12}$," *Advanced Functional Materials* 35 (2025): 2504748, https://doi.org/10.1002/adfm.202504748.

60. D. V. Semenok, D. Zhou, W. Chen, et al., "Stability and Superconductivity of Ternary Polyhydrides," *Annalen der Physik* 538 (2025): 00467, https://doi.org/10.1002/andp.202500467.

61. Z. Qiu, J. Chen, D. V. Semenok, et al., "Interlayer coupling enhanced superconductivity near 100K in $La_{3-x}Nd_xNi_2O_7$," *arXiv* (2025): 251012359.

62. I. Kantor, V. Prakapenka, A. Kantor, et al., "BX90: A New Diamond Anvil Cell Design for X-Ray Diffraction and Optical Measurements," *Review of Scientific Instruments* 83 (2012): 125102, https://doi.org/10.1063/1.4768541.

63. A. D. Grockowiak, M. Ahart, T. Helm, et al., "Hot Hydride Superconductivity Above 550 K," *Frontiers in Electronic Materials* 2 (2022): 837651.

64. V. Struzhkin, B. Li, C. Ji, et al., "Superconductivity in La and Y Hydrides: Remaining Questions to Experiment and Theory," *Matter and Radiation at Extremes* 5 (2020): 028201, https://doi.org/10.1063/1.5128736.

65. Y. L. Wu, X. H. Yu, J. Z. L. Hasaien, et al., "Ultrafast Dynamics Evidence of Strong Coupling Superconductivity in $LaH_{10\pm\delta}$," *Nature Communications* 15 (2024): 9683, https://doi.org/10.1038/s41467-024-53103-w.

66. Q. Jiang, D. Duan, H. Song, et al., "Prediction of Room-Temperature Superconductivity in Quasi-Atomic H_2-Type Hydrides at High Pressure," *Advanced Science* 11 (2024): 2405561, https://doi.org/10.1002/advs.202405561.

67. C. F. Macrae, I. Sovago, S. J. Cottrell, et al., "Mercury 4.0: From Visualization to Analysis, Design and Prediction," *Journal of Applied Crystallography* 53 (2020): 226–235, https://doi.org/10.1107/S1600576719014092.

68. R. Hrubiak, J. S. Smith, and G. Shen, "Multimode Scanning X-Ray Diffraction Microscopy for Diamond Anvil Cell Experiments," *Review of Scientific Instruments* 90 (2019): 025109, https://doi.org/10.1063/1.5057518.

69. M. A. Kuzovnikov, "Composition Estimation of Novel Lanthanum Superhydrides," a report presented at the 27th AIRAPT International Conference on High Pressure and Technology, Rio de Janeiro (Brazil), August 4–9, 2019.

70. M. A. Kuzovnikov, A. P. Drozdov, and P. Kong, "Crystal Structures of Novel Lanthanum Superhydrides," a report presented at 57th EHPRG Meeting on High Pressure Science and Technology, Prague, Czech Republic (2019).

71. M. A. Kuzovnikov, "V(P) Equations of state of Novel Lanthanum and Yttrium Superhydrides," presented at XXXVI Fortov International Conference on Interaction of Intense Energy Fluxes with Matter (ELBRUS 2021), V(P) Equations of state of Novel Lanthanum and Yttrium Superhydrides, ELBRUS (2021).

72. D. V. Semenok, I. A. Troyan, A. G. Kvashnin, et al., "Superconductivity at 253 K in Lanthanum–Yttrium Ternary Hydrides," *Materials Today* 48 (2021): 18–28, https://doi.org/10.1016/j.mattod.2021.03.025.

73. A. H. Manayil Marathamkottil, K. Wang, N. P. Salke, et al., "X-Ray-Diffraction and Electrical-Transport Imaging of Superconducting Superhydride $(La,Y)H_{10}$," *Nature Communications* 16 (2025): 11222, https://doi.org/10.1038/s41467-025-66262-1.

74. D. Zhou, D. V. Semenok, D. Duan, et al., "Superconducting Praseodymium Superhydrides," *Science Advances* 6 (2020): aax6849, https://doi.org/10.1126/sciadv.aax6849.

75. J. Du, W. Sun, X. Li, and F. Peng, "Pressure-Induced Stability and Superconductivity in LuH_{12} Polyhydrides," *Physical Chemistry Chemical Physics* 25 (2023): 13320–13324, https://doi.org/10.1039/D3CP00604B.

76. J. Bi, Y. Nakamoto, P. Zhang, et al., "Stabilization of Superconductive La–Y Alloy Superhydride with T_c Above 90 K at Megabar Pressure," *Materials Today Physics* 28 (2022): 100840.

77. W. Chen, X. Huang, D. V. Semenok, et al., "Enhancement of Superconducting Properties in the La–Ce–H System at Moderate Pressures," *Nature Communications* 14 (2023): 2660, https://doi.org/10.1038/s41467-023-38254-6.

78. O. Gunaydin-Sen, R. Achey, N. S. Dalal, A. Stowe, and T. Autrey, "High Resolution ^{15}N NMR of the 225 K Phase Transition of Ammonia Borane (NH_3BH_3): Mixed Order-Disorder and Displacive Behavior," *Journal of Physical Chemistry B* 111 (2007): 677–681, https://doi.org/10.1021/jp0649347.

79. COMSOL Multiphysics v. 6.0., wwwcomsol.com. COMSOL AB, Stockholm, Sweden.

80. A. A. Abrikosov, "The Magnetic Properties of Superconducting Alloys," *Journal of Physics and Chemistry of Solids* 2 (1957): 199–208, https://doi.org/10.1016/0022-3697(57)90083-5.

81. A. V. Sadakov, V. A. Vlasenko, I. A. Troyan, et al., "Vortex Phase Dynamics in Yttrium Superhydride YH_6 at Megabar Pressures," *Journal of Physical Chemistry Letters* 14 (2023): 6666–6671, https://doi.org/10.1021/acs.jpclett.3c01577.

82. A. V. Sadakov, V. A. Vlasenko, D. V. Semenok, et al., "Quasi-Two-Dimensional Vortex Matter in the ThH_{10} Superhydride," *Physical Review B* 109 (2024): 224515, https://doi.org/10.1103/PhysRevB.109.224515.

83. V. S. Minkov, V. Ksenofontov, S. L. Bud'ko, E. F. Talantsev, and M. I. Eremets, "Magnetic Flux Trapping in Hydrogen-Rich High-Temperature Superconductors," *Nature Physics* 19 (2023): 1293–1300, https://doi.org/10.1038/s41567-023-02089-1.

84. M. I. Eremets, V. S. Minkov, A. P. Drozdov, and P. P. Kong, "The Characterization of Superconductivity Under High Pressure," *Nature Materials* 23 (2024): 26–27, https://doi.org/10.1038/s41563-023-01769-w.

85. D. C. Cavanagh and B. J. Powell, "Fate of the Hebel-Slichter Peak in Superconductors with Strong Antiferromagnetic Fluctuations," *Physical Review Research* 3 (2021): 013241, https://doi.org/10.1103/PhysRevResearch.3.013241.

86. R. Akis and J. P. Carbotte, "Damping Effects on NMR in Superconductors," *Solid State Communications* 78 (1991): 393–396, https://doi.org/10.1016/0038-1098(91)90691-N.

87. A. B. Migdal, "Interaction Between Electrons and Lattice Vibrations in a Normal Metal," *Soviet Physics—Jetp* 7 (1958): 996–1001.

88. G. M. Eliashberg, "Interactions between Electrons and Lattice Vibrations in a Superconductor," *Soviet Physics—Jetp* 11 (1960): 696–709.

89. D. Semenok, J. Guo, D. Zhou, et al., "Evidence for Pseudogap Phase in Cerium Superhydrides: CeH_{10} and CeH9," *arXiv* (2023): 230711742v2.

90. D. V. Semenok, I. A. Troyan, A. V. Sadakov, et al., "Effect of Magnetic Impurities on Superconductivity in LaH_{10}," *Advanced Materials* 34 (2022): 2204038, https://doi.org/10.1002/adma.202204038.

91. Y. Song, C. Ma, H. Wang, et al., "Room-Temperature Superconductivity at 298 K in Ternary La-Sc-H System at High-Pressure Conditions," *arXiv* (2025): 251001273.

Supporting Information

Additional supporting information can be found online in the Supporting Information section.

Supporting File: advs74245-sup-0001-SuppMat.docx.